Journal of Hydrology 603 (2021) 126974

Contents lists available at ScienceDirect

Journal of Hydrology

journal homepage: www.elsevier.com/locate/jhydrol

Isotopic kinetic fractionation of evaporation from small water bodies

Chengyu Xie [a], Wei Xiao [a,b,*], Mi Zhang [a], Shoudong Liu [a], Yufei Qian [a], Hao Zhu [a], Zhen Zhang [a], Qiang Liu [a], Yongbo Hu [a], Jingyuan Wang [c], Xuhui Lee [d,*]

[a] Yale-NUIST Center on Atmospheric Environment, International Joint Laboratory on Climate and Environment Change (ILCEC), Nanjing University of Information Science and Technology, Nanjing, Jiangsu Province 210044, China
[b] Key Laboratory of Meteorological Disaster, Ministry of Education and Collaborative Innovation Center on Forecast and Evaluation of Meteorological Disasters, Nanjing University of Information Science and Technology, Nanjing, Jiangsu Province 210044, China
[c] Key Laboratory of Ecosystem Network Observation and Modeling, Institute of Geographic Sciences and Natural Resources Research, Chinese Academy of Sciences, Beijing 100101, China
[d] School of the Environment, Yale University, New Haven, Connecticut 06511, USA

ARTICLE INFO

Keywords:
Kinetic fractionation
Oxygen and hydrogen isotopes
Local evaporation line
Small water bodies

ABSTRACT

The primary objective of this study is to investigate the kinetic fractionation of evaporation of small water bodies. The experiments were performed in outdoor conditions using two evaporation pans and a small fishpond. The work is motivated in part by the high sensitivity of lake evaporation derived from isotopic mass balance to the strength of the kinetic effect. Results show that the kinetic factor ε_k for the oxygen isotopes is inversely related to the water-to-air temperature gradient, indicating the important role of convective turbulence in kinetic fractionation of evaporation. Although the measured ε_k displays a weak correlation with the slope of the local evaporation line (LEL), by replacing the default ε_k value of 14.2 ‰ (for ^{18}O) commonly adopted for lake studies, it greatly improves the performance of a theoretical LEL model. The ε_k data in this study and reported by other authors do not support the hypothesis that ε_k decreases with increasing lake size. The overall mean ε_k is 9.7 ‰ for ^{18}O and 8.5 ‰ for ^{2}H, based on nine outdoor experimental results.

1. Introduction

Small lakes and ponds (area < 1 km^2) are widely distributed in the terrestrial environment (Verpoorter et al., 2014; Messager et al., 2016). They comprise over 99 % of the 300 million water bodies in the world and occupy about half of the total water area on land (Downing et al., 2006). These small water bodies are highly dynamic over time (Berg et al., 2016; Finger Higgens et al., 2019; Maberly et al., 2020) and are vulnerable to natural and anthropogenic perturbations (Habets et al., 2018). They serve important society and ecosystem functions, such as modulation of river discharge (Fowler et al., 2015), supply of household water consumption (Alvarez et al., 2008; Carvajal et al., 2014; Yao et al., 2018), and amphibian habitats (Scheffer et al., 2006; Wang et al., 2018). Accurate quantification of their evaporative water loss to the atmosphere is an important step towards a better prediction of how this water resource may be affected by environmental changes.

Unlike land evaporation, lake evaporation occurs without water limitation and can be calculated with the Priestley-Taylor model of potential evaporation (Priestley and Taylor, 1972). For large lakes, this model performs quite well (Stewart and Rouse, 1976; Guo et al., 2015; Assouline et al., 2016; Xiao et al., 2020). For small lakes with short fetch, the model suffers from low biases because the sensible heat advected from the adjacent land provides additional energy to fuel the evaporation. A field experiment at a small subarctic lake shows that the bias can be as large as 40 % on the daily time scale (Bello and Smith, 1990).

Owing to the advection effect, the Monin-Obukhov similarity does not hold in the atmospheric surface layer over small lakes, and the gradient-diffusion technique is not recommended for measuring lake evaporation (Assouline et al., 2016). Another measurement technique is eddy covariance. But a successful eddy covariance application also requires that the fetch is sufficiently large so that the eddy covariance flux footprint falls within the boundary of the targeted water surface. For a small water body, this fetch requirement is easily violated if the eddy covariance sensor is too high above the surface (Xiao et al., 2018; Zhao et al., 2019). A very low observation height is necessary to reduce the flux footprint and to avoid the interference by water vapor evaporated

* Corresponding authors at: Yale-NUIST Center on Atmospheric Environment, Nanjing University of Information Science and Technology, Nanjing, Jiangsu Province 210044, China (W. Xiao); School of the Environment, Yale University, New Haven, Connecticut 06511, USA (X. Lee).
E-mail addresses: wei.xiao@nuist.edu.cn (W. Xiao), xuhui.lee@yale.edu (X. Lee).

https://doi.org/10.1016/j.jhydrol.2021.126974
Received 19 November 2020; Received in revised form 21 July 2021; Accepted 13 September 2021
Available online 20 September 2021

outside of the water body. But because eddies that dominate water vapor transport are small at a low measurement height (Kaimal and Finnigan, 1994), high-frequency loss is a large source of the flux measurement error (Moore, 1986).

Alternatively, lake evaporation can be determined with isotopic mass conservation (Zuber, 1983; Gat et al., 1994; Jasechko et al., 2014). In this application, the evaporation rate is obtained by combining the measurement of isotopic compositions of inflow, outflow and lake water at the start and end of an observational period, with the isotopic composition of evaporation δ_E calculated with the Craig-Gordon (CG) model. One of the most critical parameters for the CG model calculation is the kinetic fractionation factor (ε_k), or the isotope relative enrichment due to molecular diffusion. Xiao et al. (2017) showed that at Lake Taihu, the lake evaporation estimate is 70 % higher if they used the ε_k value of about 7.2 ‰ from an ocean evaporation parameterization (OS) than if they used the ε_k value of 14.2 ‰ (for ^{18}O) based on a default lake parameterization (LK). They found that the annual lake evaporation estimated with the OS parameterization agrees well with the water vapor flux measured with an in-situ eddy covariance instrument and that the CG-calculated δ_E produces a local evaporation line slope in agreement with the observed value.

The OS and LK ε_k parameterizations invoke different assumptions about the role of turbulence in water vapor diffusion in the atmospheric surface layer above the lake. If the diffusion pathway is fully turbulent, no kinetic effect exists, and ε_k is zero. At the other limit, if the diffusion is fully molecular, ε_k will have the highest value of 28.4 ‰ (for ^{18}O) which is the ratio, expressed in delta notation, of the molecular diffusivity of the lighter $H_2{}^{16}O$ molecule to that of the heavier $H_2{}^{18}O$ molecule in air. The LK parameterization assumes that turbulence reduces the kinetic effect of lake evaporation by half from the molecular limit (Gonfiantini, 1986; Gibson et al., 2016; Arnoux et al., 2017). In the OS parameterization, the kinetic effect is weakened further, presumably because of stronger atmospheric turbulence over the open ocean than over inland waters (Merlivat and Jouzel, 1979; Benetti et al., 2014).

In addition to Xiao et al. (2017), the field experiment performed at an ephemeral lake (Lake Gara Diba; initial size 160 m^2; Fontes and Gonfiantini, 1967) also supports use of a low ε_k value. By optimizing a unified CG model against the lake isotopic data obtained by Fontes and Gonfiantini (1967), Gonfiantini et al. (2018) found an ε_k value of 8.52 ‰ for ^{18}O. However, these two studies are not free of drawbacks. In the case of Gonfiantini et al. (2018), the vapor isotopic composition, a critical input variable of the CG model, was not measured at Lake Gara Diba but was given a somewhat arbitrary guess value. In the case of Xiao et al. (2017), δ_E was determined with the gradient-diffusion technique which requires that the diffusion of the $H_2{}^{18}O$ and $H_2{}^{16}O$ molecules is in perfect compliance with the Monin-Obukhov similarity. Furthermore, for large lakes such as Lake Taihu (area 2400 km^2), levels of wind and turbulence are high due to large open fetch conditions. It is possible that the kinetic factor is higher for small lakes due to weaker winds. In a recent study, Gonfiantini et al. (2020) have shown that in high wind conditions, the isotopic behavior of evaporating waters may deviate significantly from the CG model prediction, possibly due to different kinetics of breaking the hydrogen bonds of liquid water at the water–air interface.

The current study is motivated by the question of what ε_k value is most appropriate for evaporation of small water bodies. Its objectives are (1) to measure the ε_k of evaporation of small water bodies for the oxygen isotopes, (2) to investigate the relationship between ε_k and the slope of the local evaporation line (LEL), and (3) to test the hypothesis that the strength of the kinetic effect decreases with increasing lake size. The outdoor experimental determination of ε_k was carried out using a fishpond and two evaporation pans as proxies for small lakes. The present experiment was designed to overcome the limitations of past studies. The δ_E was determined from the first principle (mass conservation) and therefore assumptions implicit in the gradient diffusion method of Xiao et al. (2017) were avoided. The vapor isotopic composition was measured directly at high temporal resolutions that matched those of other driving variables of the CG model. Because these water bodies are small (surface area from 0.13 m^2 to 6900 m^2), their influence on the overlaying air was negligible. At large lakes, surface evaporation and the overlaying air are interactive (Feng et al., 2016). Evaporation will modify the humidity and the vapor isotopic composition as the air moves across the lake. The humidity and vapor isotopic composition changes in turn will modify surface evaporation and its isotopic composition. Such interactions are a source of uncertainty in CG model calculations.

2. Materials and methods

2.1. Experimental site and instruments

The goal of the field experiment was to determine ε_k by inverting the isotopic mass balance equation. Isotope and micrometeorological data were collected for a fishpond and two evaporation pans. The fishpond, located in Anhui Province, China (118.25 °E and 31.97 °N), had an area of 6900 m^2 and average depth of 2.1 m. A total of six trials were conducted, with a duration of 10 to 50 days (Table 2). During the trials, a water sample was collected once a day at the 20-cm depth. Micrometeorological variables, measured at half-hourly intervals, included the four components of the net radiation (model CNR4, Kipp & Zonen B. V., Delft, the Netherlands), the profile of water temperature at depths of 20, 50, and 80 cm (temperature probes model 109-L, Campbell Scientific, Inc., Logan, Utah, USA), air temperature and humidity (model HMP155A, Vaisala, Inc., Helsinki, Finland) at a height of 2 m above the surface, wind speed and wind direction (model 05103, R M Young, Inc., Traverse City, Michigan, USA) at a height of 3 m, and eddy fluxes of water vapor, sensible heat and momentum (sonic anemometer/thermometer, model CSAT3A, Campbell Scientific, Inc.; open-path CO_2/H_2O infrared gas analyzer, model EC150, Campbell Scientific, Inc.) at a height of 2 m. Rainfall was observed at a weather station belonging to the Quanjiao Meteorological Bureau about 12 km from the observation site. Rainfall samples were collected at the site for individual precipitation events for isotopic analysis. The water surface temperature was inverted from the outgoing and incoming longwave radiation using the Stefan-Boltzmann Law with an emissivity of 0.97.

To maintain a sufficient water level, local famers pumped 412 and 634 m^3 water from a canal into the fishpond during fishpond trials F1 and F2, respectively. A sample was collected from the pumped water for isotopic analysis.

Two evaporation pans (WMO type E601 with 61.8 cm diameter and type ϕ20 with 20 cm diameter) were installed next to the fishpond. They were partially buried in the soil to help reduce temperature fluctuations. Their bottom interiors were painted black to promote absorption of solar radiation and convective mixing of the water column. The water surface temperature was measured with an infrared thermometer (model SI-111, Campbell Scientific, Inc). Water temperature was also measured at 2 cm below the surface (model 109-L, Campbell Scientific, Inc). Three experimental trials, each lasting 13 to 20 days, were made with the big pan, and six trials, each lasting 4 to 10 days, were made with the small pan. The initial water mass was about 100 kg and the final mass was about 90 kg in the big pan trials. The initial and the final mass in the small pan trials were about 3 kg and 2 kg, respectively. A small sample (5 mL) was collected each day for isotopic analysis. The evaporation rate was determined daily by measurement of the water level and corrected for the removal of water samples. The pans were covered during rain events. For the big pan, the water surface was 26.73 cm to 31.99 cm below the top edge. For the small pan, the distance ranged from 1.53 cm to 4.95 cm.

The Craig-Gordon model calculation requires measurement of the isotopic composition of water vapor. This measurement was made in-situ with a water vapor isotope analyzer (model 911-0004, Los Gatos Research, Mountain View, CA, USA) located at a distance of 100 m from

the fishpond. The analyzer inlet was positioned at a height of 9 m above the water surface. The analyzer sampling frequency was 1 Hz and the data were averaged to 60-min intervals. Calibration of the vapor isotope measurement was made with a vapor source supplied with working liquid water standards (model 908-0003-9002, Los Gatos Research) traceable to the VSMOW scale. The liquid water standards had delta values in the range of −8.7 to −3.0 ‰ for $\delta^{18}O$ and −59.4 to −26.2 ‰ for $\delta^{2}H$. The calibration was performed at five humidity levels that were adjusted dynamically to bracket the ambient humidity (Xiao et al., 2017).

Isotopic analysis of liquid water samples, including rainwater, irrigation water, fishpond water, and evaporation pan water, was made with a liquid water isotope analyzer (model DLT-100, Los Gatos Research) in the Key Laboratory of Ecosystem Network Observation and Modeling, Chinese Academy of Sciences. The analyzer was calibrated against 3 working standards traceable to the VSMOW scale ($\delta^{2}H/\delta^{18}O$: −79.6/−11.04, −49.2/−7.81, −9.9/−2.99 ‰). All liquid water samples were sealed and placed in a refrigerator at 4 °C before analysis.

All isotope values are expressed as delta scale δ (‰) = $[(R_{sample}/R_{VSMOW})–1] \times 1000$, where R is the $^{2}H/^{1}H$ or $^{18}O/^{16}O$ ratio and R_{VSMOW} are 0.00015576 for $^{2}H/^{1}H$ and 0.0020052 for $^{18}O/^{16}O$. The analytical uncertainty of the liquid water isotope measurement is 0.3 ‰ for $\delta^{2}H$ and 0.1 ‰ for $\delta^{18}O$, and the uncertainty of the vapor isotope measurement after calibration is 2 ‰ for $\delta^{2}H$ and 0.2 ‰ for $\delta^{18}O$.

2.2. Isotope mass balance analysis

We used the mass balance equations to obtain the isotopic composition of evaporation δ_E and the mean evaporation rate E_t for each experimental trial described above. The complete expression of mass balance of a water body is

$$I + P = O + S + E + dV \quad (1)$$

where I is inflow water, P is precipitation, O is outflow water, S is the amount of water sample removed for isotopic analysis, E is evaporation water loss, and dV is the change of water amount during the experimental period. The isotopic mass balance equation is

$$I\delta_I + P\delta_P = O\delta_O + S\delta_S + E\delta_E + d(V\delta_L) \quad (2)$$

where δ is isotopic composition of ^{2}H or ^{18}O in delta-notation, and subscripts I, P, O, S, E and L denote inflow, precipitation, outflow, sampled water, evaporated water, and liquid water in the fishpond or the evaporation pans, as defined in Table 1. For the evaporation pans, inflow and outflow were zero, and precipitation input was also zero. For the fishpond, S was negligible, outflow was zero because no drainage occurred during the experimental trials, and I was the water input via pumping during F1 and F2 and zero for other trials.

All the terms in Eqs. (2) and (3) except E and δ_E were measured experimentally. The total amount of evaporation E was determined from Eq. (1) and was converted to evaporation rate E_t in units of g m^{-2} s^{-1}. The isotopic composition of evaporation δ_E was determined from Eq. (2).

2.3. Experimental determination of the kinetic factor: The mass balance approach

We combined the δ_E obtained from the isotopic mass balance with the Craig-Gordon model (Craig and Gordon, 1965) to quantify the kinetic factor for ^{18}O. According to the model, the hourly isotopic composition of evaporation is given by

$$\delta_E^{'} = \frac{\alpha_{eq}^{-1}\delta_L - h\delta_V - \varepsilon_{eq} - (1-h)\varepsilon_k}{1 - h + 0.001(1-h)\varepsilon_k} \quad (3)$$

where h is relative humidity (in fraction) in reference to the saturated vapor pressure at the water surface, δ_V is isotopic composition of water vapor, δ_L is isotopic composition of liquid water in the evaporation pans or the fishpond, α_{eq} (>1) is the equilibrium fractionation factor, $\varepsilon_{eq} = 10^{3}(1–1/\alpha_{eq})$ is the equilibrium factor in delta notation (‰), and ε_k is isotopic kinetic fractionation factor (‰). The prime symbol indicates that the calculated isotopic composition of evaporation is an hourly value, to distinguish it from the whole-trial mean δ_E from Eq. (2). In Eq. (3), h and T_s were means of two 30-min measurements, α_{eq} and ε_{eq} were determined as a function of the water surface temperature, δ_L was linearly interpolated to hourly intervals from the daily isotope measurement of the liquid sample. But ε_k is an unknown parameter to be determined by an optimization method described below (Supplementary Figure S1).

Eq. (3) helps to clarify the definition of the kinetic factor used in the present study: it is a property intrinsic to atmospheric flow and is not related to the status of atmospheric humidity. The total kinetic effect is given by $(1 – h)\ \varepsilon_k$.

The bulk aerodynamic method was used to determine a weighting factor for the fishpond trials. This method expressed the hourly evaporation rate as

$$E_t^{'} = \rho_a C_E u(q_s - q_a) \quad (4)$$

where ρ_a is air density, C_E is the transfer coefficients for moisture, u is wind speed, and q_s and q_a are the specific humidity at the surface and at

Table 1
List of symbols.

Variables	Description
I	Inflow water (kg)
P	Precipitation (kg)
O	Outflow water (kg)
S	Amount of water sample removed for isotopic analysis (kg)
E	Evaporation water loss (kg)
E_t	Evaporation rate (g m^{-2} s^{-1}), converted from evaporation E according to Eq. (1)
dV	The change of water amount during the experimental period (kg)
δ	Isotopic composition of sample water relative to a standard of known composition (‰); for ^{2}H, it represents $^{2}H/^{1}H$; for ^{18}O, it represents $^{18}O/^{16}O$
δ_I	Isotopic composition of inflow water (‰)
δ_P	Isotopic composition of precipitation (‰)
δ_O	Isotopic composition of outflow water (‰)
δ_S	Isotopic composition of water sample (‰)
δ_E	Isotopic composition of evaporated water (‰), a mean value for the whole experiment
δ_E'	Isotopic composition of evaporated water (‰), hourly value calculated by Eq. (3)
δ_L	Isotopic composition of liquid water in the fishpond or the evaporation pans (‰)
δ_V	Isotopic composition of water vapor (‰)
h	Relative humidity (in fraction) in reference to the saturated vapor pressure at the water surface
f	Residual water fraction (in fraction), calculated as m_f/m_0
T_s	Water surface temperature (°C)
α_{eq}	The equilibrium fractionation factor (>1), calculated from T_s
ε_{eq}	The equilibrium factor (‰) (>0), $\varepsilon_{eq} = 10^{3}(1 - 1 / \alpha_{eq})$
ε_k	The isotopic kinetic fractionation factor (‰)
E_t'	Hourly evaporation rate (g m^{-2} s^{-1}), calculated from Eq. (4)
ρ_a	Air density (kg m^{-3})
C_E	Transfer coefficient for moisture
u	Wind speed (m s^{-1})
q_s	The specific humidity at the surface (kg kg^{-1})
q_a	The specific humidity at the reference height (kg kg^{-1})
$\rho_a u(q_s - q_a)$	Evaporation-flux weighting factor
E_i	The actual daily evaporation amount observed on day i (kg)
C_i	A daily correction coefficient calculated by Eq. (6)
r_i	Diffusion resistance of the heavier molecule
r	Diffusion resistance of the lighter molecule
D	The molecular diffusivity of major water isotopic species in air
D_i	The molecular diffusivity of minor water isotopic species in air
n	Aerodynamic parameter, ranges between 0 under fully turbulent conditions and 1 if the diffusion is completely molecular

Table 2
Summary of environmental variables. Here, δ_V (vapor isotopic composition), u (wind speed), u_* (friction velocity), h (relative humidity in reference to water surface temperature), T_a (air temperature) and T_s (water surface temperature) are weighted mean values. M is water mass, δ_L is isotopic composition of liquid water, E_t is evaporation rate, and subscript 0 and f denote initial and final value, respectively. The wind speed range is given in the parentheses.

Trial	Period	T	^{2}H			^{18}O			M_0	M_f	f	u	u_*	h	T_a	T_s	E_t
			$\delta_{L,0}$	$\delta_{L,f}$	δ_V	$\delta_{L,0}$	$\delta_{L,f}$	δ_V									
		day	‰	‰	‰	‰	‰	‰	kg	kg		m s^{-1}	m s^{-1}		°C	°C	g m^{-2} s^{-1}
Small evaporation pan																	
S1	05/09–05/17/2017	8.1	–46.8	5.3	–83.7	–6.7	3.8	–13.1	3.18	1.63	0.51	1.58 (0.12–3.85)	0.18	0.40	25.96	28.72	0.103
S2	05/22–05/27/2017	5.0	–45.9	–12.3	–80.8	–5.0	0.2	–12.7	2.99	1.91	0.64	1.21 (0.14–4.10)	0.17	0.37	27.14	31.05	0.121
S3	07/18–07/22/2017	4.0	–40.0	–20.9	–101.8	–6.6	0.0	–14.3	2.99	1.84	0.62	1.65 (0.35–2.58)	0.14	0.47	33.10	36.65	0.100
S4	07/23–07/28/2017	4.7	–36.9	–9.8	–78.9	–5.6	0.0	–11.2	3.07	1.77	0.58	1.87 (0.20–3.16)	0.10	0.46	35.13	40.70	0.096
S5	07/28–08/02/2017	4.9	–37.9	–27.3	–97.9	–6.4	–3.0	–13.7	2.97	2.31	0.78	2.86 (1.00–6.05)	0.22	0.62	32.96	35.51	0.102
S6	10/31–11/10/2017	10.3	–35.2	–6.6	–122.9	–5.2	–0.1	–20.0	3.14	1.86	0.59	2.54 (0.03–5.46)	0.22	0.55	15.91	18.15	0.033
Big evaporation pan																	
B1	05/09–05/29/2017	19.7	–45.9	–23.1	–83.1	–6.8	–1.9	–12.9	110.75	87.63	0.79	1.66 (0.10–4.10)	0.19	0.45	25.27	27.76	0.064
B2	07/18–08/01/2017	14.7	–40.1	–28.7	–92.5	–6.6	–3.5	–13.1	106.15	89.39	0.84	1.86 (0.20–6.05)	0.14	0.55	33.38	34.70	0.056
B3	10/31–11/13/2017	13.3	–46.6	–38.1	–126.9	–7.0	–5.2	–20.6	94.01	87.58	0.93	2.29 (0.03–5.46)	0.19	0.57	14.40	14.65	0.022
Fishpond																	
F1	05/09–05/29/2017	19.8	–15.7	–10.5	–82.8	–1.5	–1.0	–12.9				1.85 (0.10–4.10)	0.21	0.49	24.69	25.77	0.047
F2	07/18–08/01/2017	13.8	–22.0	–20.5	–97.6	–2.3	–1.9	–13.7				2.28 (0.20–5.34)	0.19	0.55	33.05	34.62	0.075
F3	07/30–08/13/2018	14.1	–13.8	–16.3	–91.8	–1.0	–0.7	–13.5				1.59 (0.19–3.98)	0.17	0.58	31.34	33.63	0.051
F4	08/29–10/06/2018	38.3	–24.0	–20.8	–104.9	–1.6	–1.1	–15.5				1.92 (0.21–4.31)	0.18	0.56	24.96	26.68	0.056
F5	10/11–11/30/2018	50.0	–20.9	–17.1	–103.9	–0.8	–0.2	–16.5				2.41 (0.06–5.78)	0.20	0.54	16.05	16.80	0.039

the reference height, respectively. So the parameter group $\rho_a u(q_s - q_a)$ was used as evaporation-flux weighted factor. The Craig-Gordon model calculation was upscaled to give the δ_E of the whole experimental trial as,

$$\delta_E = \frac{\sum\left(\delta_E^{'} \times \rho_a u(q_s - q_a)\right)}{\sum \rho_a u(q_s - q_a)} \quad (5)$$

Eq. (5) makes the assumption that C_E is invariant with time. The evaporation-flux weighting factor $\rho_a u(q_s - q_a)$ was calculated on an hourly scale. This weighting factor is essentially a bulk parameterization for open-water evaporation whereby the rate of evaporation is proportional to wind speed and to the vapor concentration difference between the water surface and a reference height in the surface layer.

The kinetic factor ε_k was determined using a numerical optimization method with Eqs. (3)-(5). The optimization aimed to achieve a perfect match between δ_E calculated from these equations and the δ_E determined from the isotopic mass conservation (Eq. (2)). The method yielded a solution of ε_k.

The bulk relationship was also used to obtain the evaporation-flux weighted factor for the pan experiments (Supplementary Figure S2). However, we found that the transfer coefficient showed day-to-day variations. To account for these variations, we included a daily correction coefficient C_i so the weighting becomes $C_i \rho_a u(q_s - q_a)$. The coefficient C_i is given by

$$C_i = \frac{E_i}{\sum \rho_a u(q_s - q_a)} \quad (6)$$

where E_i is the actual daily evaporation amount observed on day i. The ε_k value was also found through the optimization method with Eqs. (3)–(5) except that the weighting factor was calculated with a correction coefficient C_i.

2.4. Experimental determination of the kinetic factor: The unified CG model approach

The kinetic factor was also determined with the unified CG model of Gonfiantini et al. (2018). This model combines the CG model with the isotopic mass balance equation into an integral form and predicts δ_L as a function of the residual liquid water fraction. In this model, water temperature, humidity, vapor isotopic composition and initial δ_L are known variables. The kinetic effect appears in this model as a tunable turbulence parameter n.

The n value was determined for each pan experiment by optimizing the model predicted δ_L against the observed δ_L. The goal of the optimization was to minimize the sum of squared errors of δ_L. All the input variables were flux-weighted mean values as described above.

The relationship between n and r_i/r, or the ratio of the diffusion resistance of the heavier $H_2{}^{18}O$ molecule (r_i) to that of the lighter $H_2{}^{16}O$ molecule (r), is given by

$$\frac{r_i}{r} = \left(\frac{D}{D_i}\right)^n \quad (7)$$

where D and D_i denote the molecular diffusivity of major and minor water isotopic species in air, respectively. The n value ranges between 0 under fully turbulent conditions and 1 if the diffusion is completely molecular. The kinetic factor ε_k was obtained from the optimized n from

the following equation (Gonfiantini, 1986)

$$\varepsilon_k = n\left(\frac{D}{D_i} - 1\right)10^3 \quad (8)$$

The diffusivity ratio D_i/D is set to the value of 0.9723 for ^{18}O and 0.9755 for ^{2}H (Merlivat, 1978; Hellmann and Harvey, 2020), giving an ε_k of 28.4 ‰ for ^{18}O and 25.0 ‰ for ^{2}H at $n = 1$.

In principle, the mass balance and the unified CG methods can used to constrain the kinetic factor for ^{2}H. To our best knowledge, no published studies have used ^{2}H data alone to determine the kinetic factor in outdoor conditions. There may be two reasons for this. First, the ^{2}H fractionation of water evaporation in natural conditions is dominated by the equilibrium effect. At 20 °C, the equilibrium fractionation factor (ε_{eq}) for ^{18}O is 9.4 ‰, which is comparable in magnitude to the kinetic factor. But ε_{eq} for ^{2}H (74.3 ‰) is an order of magnitude larger. The δ^2H of evaporation is not sensitive to the kinetic effect (Xiao et al., 2017). The lack of sensitivity makes it difficult to obtain an accurate estimate of the kinetic factor from the measured δ^2H of evaporation. Second, measurement errors for ^{2}H are generally larger than for ^{18}O. In the present study, the uncertainty of the liquid water delta is 0.3 ‰ for ^{2}H, which is three times that for ^{18}O (0.1 ‰). The uncertainty of the vapor delta is 10 times larger for ^{2}H (2 ‰) than for ^{18}O (0.2 ‰). In the following, we only report the result on the turbulent parameter n using the ^{18}O data. Although the ^{2}H data was not used for the determination of n, it was included in the evaluation of the relationship between the LEL slope and kinetic fractionation (Section 4.3).

3. Results

Table 2 summarizes the mean environmental conditions for all the experimental trials. The experiments were conducted in warm seasons, with the water temperature ranging from 14.7 °C to 40.7 °C. The wind speed during these times ranged from 1.21 m s^{-1} to 2.86 m s^{-1}. The δ_V varied in the range of –126.9 ‰ to –78.9 ‰ for ^{2}H and –20.6 ‰ to –11.2 ‰ for ^{18}O, which are typical of the warm season values in eastern China (Wen et al., 2008; Xiao et al., 2017). The initial δ_L of the pan experiments was on average –41.7 ‰ for ^{2}H and –6.2 ‰ for ^{18}O, which is lower than that of the fishpond water (average –19.3 ‰ for ^{2}H and –1.5 ‰ for ^{18}O). The relative humidity referenced to the water surface temperature varied in a range of 0.37 to 0.62.

Figure 1 provides an example of hourly time series of the driving variables (panels a, b and d) of the Craig-Gordon model and time series of the model-calculated hourly $\delta^{18}O$ values of evaporating vapor (δ_E') for Experiment S2. The δ_E' result shown here is given with the optimized ε_k of 6.01 ‰ for ^{18}O. The $\delta^{18}O$ value of the pan water (δ_L) was continuously enriched over time. As a result, δ_E' increased progressively from the initial value of –20.1 ‰ to –13.1 ‰ at the end of the experiment. The relative humidity (h) showed strong diurnal variations, which mirrored the variations in the water surface temperature (T_s), resulting in lower δ_E' at night than during the day. The daytime observations were weighted much more heavily than the nighttime values (panel e). With the optimized ε_k, the flux-weighted mean isotopic composition of evaporation was –17.0 ‰, matching exactly the δ_E obtained from the isotopic mass balance calculation.

Figure 2 is an example showing the application of the unified CG model to Experiment S1. The optimization yielded the best estimate of 0.25 for n. According to Eq. (8), the best estimate of ε_k for this experiment is 7.10 ‰.

Figure 3 compares ε_k value obtained with isotopic mass balance that from the unified CG model. In general, the ε_k value from isotopic mass balance agrees very well with the ε_k value from the unified CG model if the unified CG used flux-weighted mean values for its input variables (black squares; linear correlation $r = 0.99$, confidence level $p < 0.001$). In the following, unless stated otherwise, we will restrict our analysis to the isotopic mass balance data.

The results of all the experimental trials are summarized in Table 3. Here, the ^{18}O δ_E value was obtained from optimizing the Craig-Gordon model calculation against the δ_E from the isotopic mass balance, and the turbulence parameter n was obtained from Eq. (8). The δ_E shows a large range of variation, with the lowest value (–31.8 ‰) observed in experiment trial B3 with the big evaporation pan and highest value (–7.3 ‰) during F4 with the fishpond. The experimental trial S6 with the small pan experienced similar environmental conditions as trial B3 as they took place at about the same time (Table 2), but the δ_E of S6 was much higher (–13.1 ‰). A significant and negative correlation was found between δ_E (^{18}O) and ε_k (linear correlation $r = -0.69$, $p < 0.01$), confirming that a stronger kinetic effect will cause more depletion of ^{18}O in the evaporated water. The correlation between δ_E and other variables shown in Table 2 was not significant. A multivariate stepwise regression reveals that ε_k, ε_{eq}, δ_L and δ_V could explain 99 % of the δ_E variations shown in

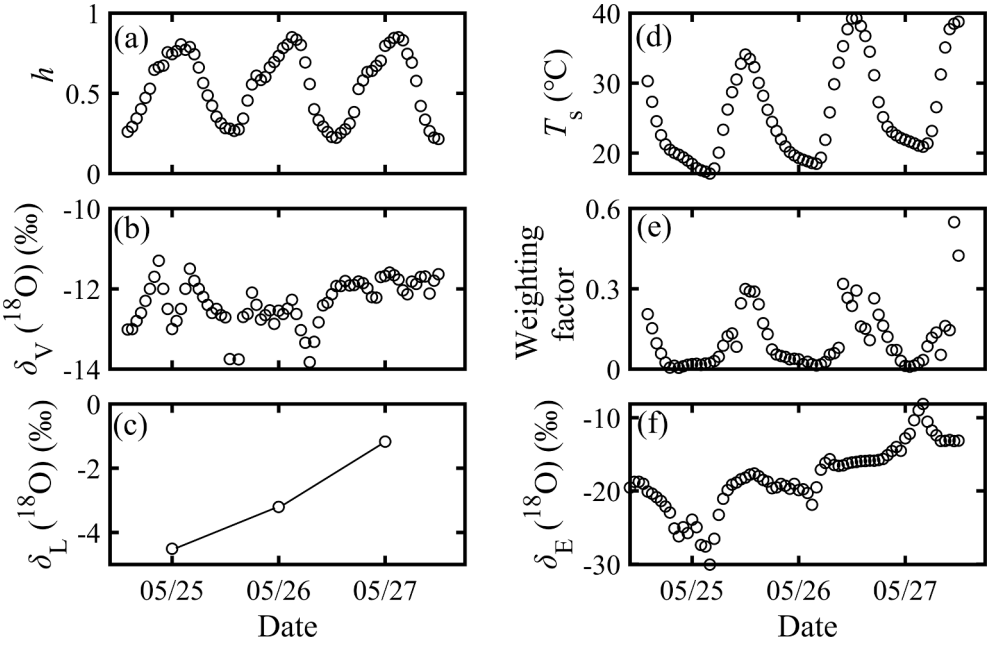

Fig. 1. Time series of environmental variables during Experiment S2.

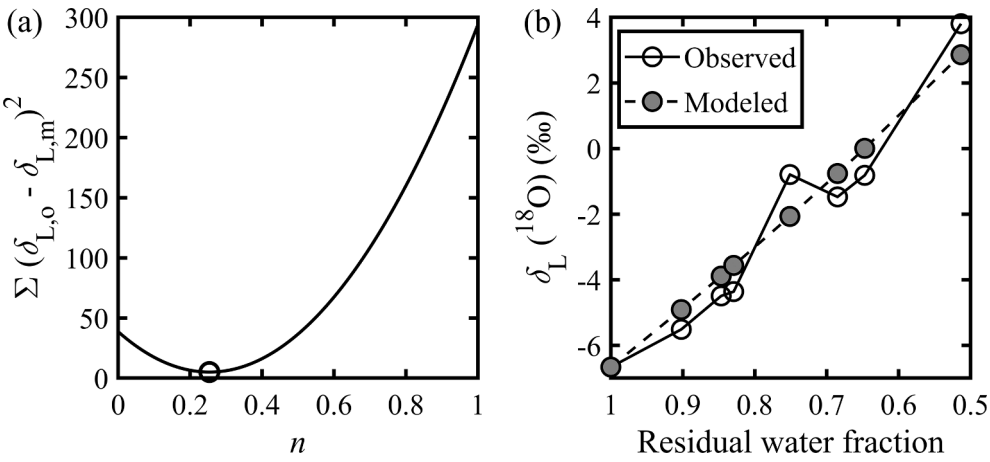

Fig. 2. Application of the unified Craig-Gordon model to Experiment S1. (a) Sum of squared errors of model-predicted δ_L versus turbulence parameter n; (b) Comparison of observed δ_L with model-predicted δ_L using the optimized n value of 0.25 (or ε_k of 7.10 ‰).

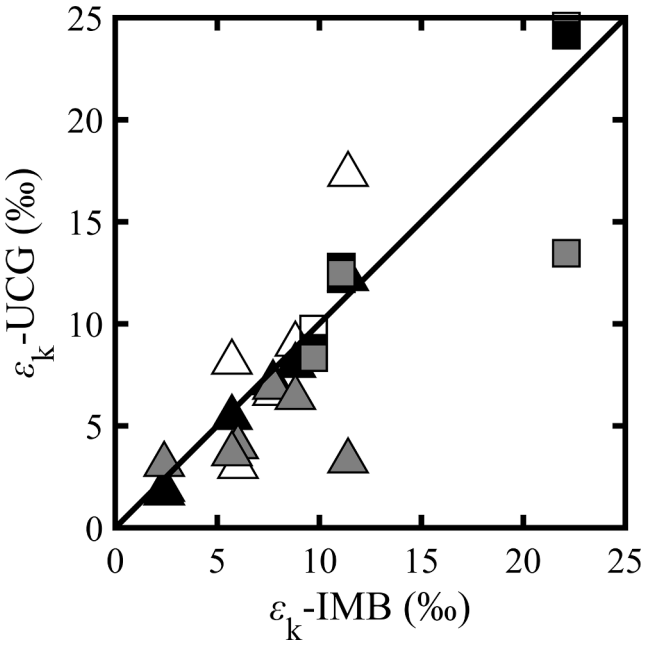

Fig. 3. Comparison of the ^{18}O kinetic factor determined with the isotopic mass balance (IMB) and that determined with the unified Craig-Gordon model (UCG) for the pan experiments. Triangles represent the small pan and squares represent the big pan. UCG calculations were performed with flux-weighted variables (solid symbols), algebraic mean input variables (open symbols), and flux-weighted variables except that the vapor delta was equilibrium value with local precipitation (grey symbols).

Table 2 and that flux-weighted relative humidity was excluded by the stepwise procedure.

The kinetic factor ε_k varied in a broad range, from 2.40 ‰ (experimental trial S4) to 22.10 ‰ (experimental trial B3), indicating a varying role of turbulence in the kinetic fractionation among these experiments. The kinetic factor showed a strong negative correlation with the water-to-air temperature difference $T_s - T_a$ ($r = -0.67$, $p < 0.01$; Fig. 4). Additionally, ε_k was negatively correlated with water surface temperature T_s ($r = -0.67$, $p < 0.01$) and the mean evaporation rate E_t ($r = -0.76$, $p < 0.01$). However, T_s and E_t were both positively correlated with $T_s - T_a$ ($r = 0.68$ for T_s and $r = 0.75$ for E_t; $p < 0.01$). The most logical explanation for these correlations is that $T_s - T_a$ exerted direct control on ε_k and the correlation of ε_k with T_s or E_t arose from their covariations with $T_s - T_a$.

The mean kinetic factor measured in this study was 7.0 ± 3.1 ‰ with the small evaporation pan, 14.3 ± 6.8 ‰ with the big evaporation pan, and 10.2 ± 4.9 ‰ with the fishpond. If we excluded B3 (Section 3.1), the mean value for the big evaporation pan (10.4 ‰) was in better agreement with that obtained with the small evaporation pan. These values agreed better with the OS value of 8.1 ‰ calculated for the mean wind conditions during this study than with the default lake value of 14.2 ‰ (Fig. 5).

The mean ε_k values from the pan experiments was 9.44 ± 5.54 ‰ (mean ± one standard deviation) according to the IMB calculation and 9.34 ± 6.60 ‰ according to the unified CG model. A two-tailed student-t test shows that there was no significant difference between the results ($p = 0.97$, $t = 0.04$). The RMSE of two sets of ε_k values was 1.27 ‰.

4. Discussion

4.1. Uncertainty analysis

We performed Monte Carlo simulations to quantify uncertainties in the calculated ε_k. Uncertainties in input variables are provided in Supplementary Table S1. Errors in these variables were assumed to follow normal distributions and to be independent of each other. A total of 10,000 ensemble members were used for each evaporation experiment, with each member producing an ε_k value. The uncertainty in ε_k was calculated as ½ of the difference between the 75th and the 25th percentile value of the ensemble. These ε_k uncertainties are smaller than the physical range of variations shown in Table 3 and Fig. 4.

In the case of the mass balance approach, uncertainties in both the δ_E mass balance measurement and the CG calculation contributed to the uncertainty in the determination of ε_k, as shown in Fig. 6 for Experiment S1. In this figure, the solid sloped line represents the δ_E as a function of ε_k (calculated with the CG model using the measured input parameters), and the solid horizontal line represents the δ_E value of –18.0 ‰ from the isotopic mass balance (Table 3). The intercept of these two lines gives the actual ε_k (7.73 ‰, Table 3) for Experiment S1, assuming no uncertainty in either the mass balance or the CG model calculation. However, both the δ_E measurement and CG model calculation carried uncertainties (shown as the range between the paired dashed lines in Fig. 6). The overall uncertainty in ε_k was ± 0.3 ‰ according to the Monte Carlo analysis. Similar ε_k uncertainty estimates were obtained for the mass balance approach applied to the other pan experiments.

The ε_k estimates for the fishpond experiments (using the isotopic mass balance method) had an uncertainty of about 1.5 ‰. This larger uncertainty stemmed primarily from the uncertainty in the δ_E determination (uncertainty of about 1.6 ‰, which is larger than the δ_E uncertainty of 0.27 ‰ for the pan Experiment S1 shown in Fig. 6) because the

Table 3
Slope of local evaporation line (S_{LEL}, dimensionless), oxygen isotopic values of evaporating vapor δ_E (‰), turbulent parameter n (dimensionless) and kinetic factor ε_k for ^{18}O (‰). IMB: isotopic mass balance; Unified CG: unified Craig-Gordon model; SSD: sum of squared deviation (deviation of the unified CG prediction from the observed value, ‰^{2}).

Trial	S_{LEL}	δ_E	n		ε_k		SSD	
		IMB	IMB	Unified CG	IMB	Unified CG	Weighted mean method	Algebraic mean method
S1	5.10	–18.0	0.27	0.25	7.73	7.10	5.08	6.75
S2	5.64	–17.0	0.21	0.14	6.01	3.98	1.08	1.61
S3	3.16	–17.6	0.31	0.28	8.82	7.95	0.47	0.39
S4	5.02	–13.4	0.08	0.06	2.40	1.70	0.64	0.69
S5	3.47	–18.8	0.20	0.19	5.72	5.40	0.21	0.25
S6	6.25	–13.1	0.40	0.43	11.41	12.21	2.24	1.83
B1	4.48	–25.4	0.39	0.45	11.07	12.78	1.05	1.02
B2	5.03	–23.4	0.34	0.31	9.72	8.80	3.57	3.53
B3	4.34	–31.8	0.78	0.85	22.10	24.14	0.62	0.62
F1	–	–15.5	0.25	–	7.18	–	–	–
F2	–	–15.8	0.35	–	9.86	–	–	–
F3	–	–16.1	0.47	–	13.46	–	–	–
F4	–	–7.3	0.14	–	4.04	–	–	–
F5	–	–18.8	0.57	–	16.31	–	–	–

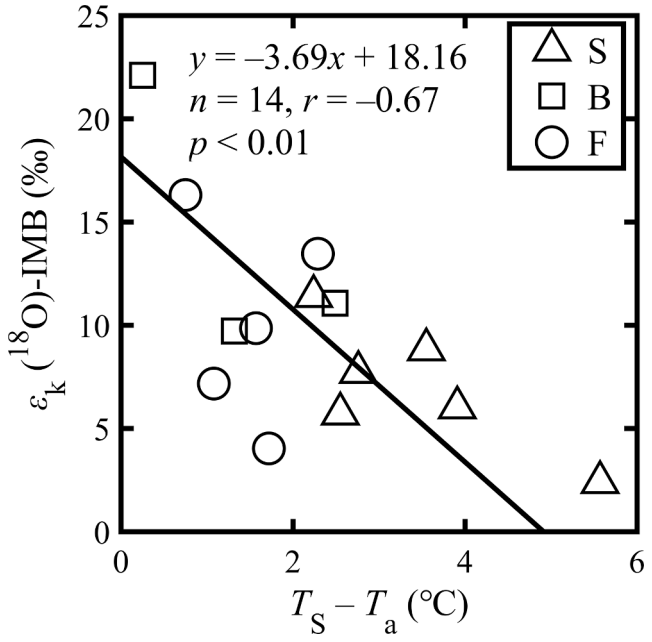

Fig. 4. Relationship between water-to-air temperature difference $T_s - T_a$ and ^{18}O kinetic fractionation factor ε_k from the isotope mass balance method. Triangles, squares and circles represent small pan, big pan and fishpond, respectively.

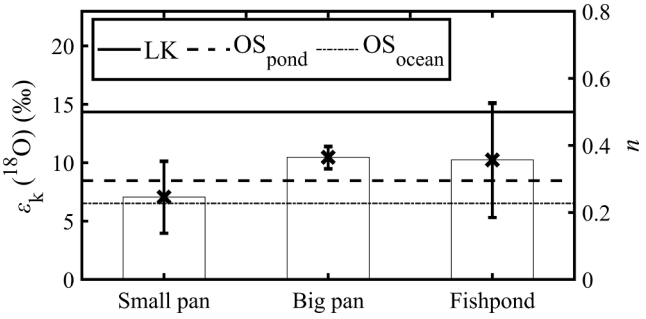

Fig. 5. Comparison of measured turbulent parameter n and kinetic factor ε_k for ^{18}O with default lake values (LK) and parameterization for ocean evaporation under smooth ocean conditions (OS_{ocean}; Araguas-Araguas et al., 2000) and the ocean parameterization using locally-observed wind speed of 1.64 m s^{-1} (OS_{pond}). Error bars are ± 1 standard deviation. B3 is excluded from this comparison.

mass balance calculation involved more input variables than for the pan experiments and because these additional variables were more uncertain than the other variables (Supplementary Table S1). In contrast, the ε_k uncertainty from the unified CG model was 5 to 10 times smaller than the uncertainty for the pan experiments from the isotopic mass balance method, indicating robustness of the unified CG model. There are two reasons for this. First, the unified CG model was constrained by the isotopic composition of the liquid water δ_L which is more accurate than δ_E (Table S1). Second, multiple δ_L measurements were used in the optimization procedure (Fig. 2 and S3), further reducing the uncertainty in the ε_k estimation.

4.2. Comparison of pan experimental data

Numerous outdoor pan experiments have been reported in the literature. The majority of these experiments aim to quantify the rate of liquid water evaporation. Some have been used to determine the isotopic composition of evaporation by adopting the traditional values of ε_k (14.2 ‰ for ^{18}O and 12.5 ‰ for ^2H; e. g., Crawford et al., 2019; Devi et al., 2015; Skrzypek et al., 2015). According to the survey by Gonfiantini et al. (2018), two pan experiments have been conducted in the past to investigate kinetic isotopic fractionation of evaporation in natural conditions. The first one was carried out by Craig et al. (1963) on the roof of a laboratory building in La Jolla, California for a duration of 16 days. The second one was carried out in an open field by Skrzypek et al. (2015) in Western Australia for a duration of 12–16 days. Recently Gonfiantini et al. (2018) used the unified CG model to constrain the turbulent parameter n with the data from these experiments. Because the isotopic ratio of water vapor was not measured (Fontes and Gonfiantini, 1967), Gonfiantini et al. (2018) approximated vapor delta with the value in equilibrium with local precipitation. This approximation is somewhat arbitrary because precipitation events were rare. However, its impact on δ_E is rather limited due to the low air humidity. In addition, algebraic mean values were used for other input variables of the model. The resulting n is 0.5 (ε_k = 14.2 ‰ for ^{18}O) for Craig's experiment and 0.4 (ε_k = 11.36 ‰ for ^{18}O) for Skrzypek's experiment. (In their original study, Skrzypek et al. (2015) used the traditional value of 14.2 ‰ for ε_k).

The current study was inspired by the work of these authors. The IRIS instrument brought two improvements to the pan experimental method. First, the vapor isotopic composition was directly measured, so the equilibrium approximation was no longer needed. Second, instead of simple algebraic averaging, flux-weighted mean values for input variables (h, ε_{eq} and δ_V) were used in the unified CG model calculation in order to account for the fact that environmental conditions during times

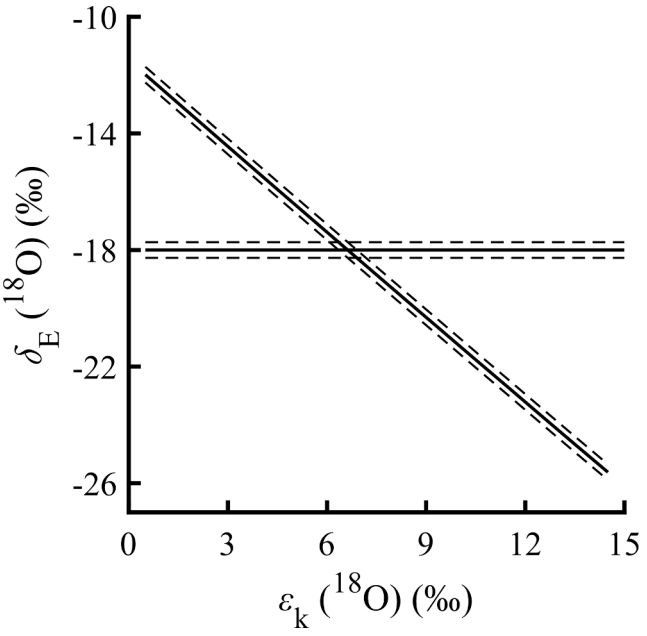

Fig. 6. Sensitivity of the isotopic value of evaporating vapor (δ_E) to the kinetic factor (ε_k) for Experiment S1. Here the solid sloped line represents the Craig-Gordon model prediction using the input variables as measured, and the solid horizontal line is the isotopic value of evaporation determined with isotopic mass balance. The paired dash lines indicate the uncertainty range (±1 standard deviation).

of higher evaporation exert a stronger influence on the cumulative fractionation of the evaporating water. With these improvements, the ε_k from the unified CG model was in excellent agreement with that obtained from isotopic mass balance, with a small root mean square error (RMSE) of 1.27 ‰ (solid symbols, Fig. 3). If simple algebraic means of the forcing variables were used for the unified CG calculation, the RMSE became larger, at 2.55 ‰ (open symbols, Fig. 3). The unified CG model was also sensitive to how the vapor delta was obtained. The amount-weighted isotopic composition of precipitation during the 2017 experimental season (May to November) was –3.38 ‰ (^{18}O). If the vapor delta value in equilibrium with the local precipitation was used instead of the observed value, the ε_k could deviate significantly from that obtained with the isotopic mass balance method, giving a large overall RMSE of 4.23 ‰ (grey symbols, Fig. 3).

Our experimental study seems to be the first to provide direct evidence for the role of turbulence in kinetic fractionation in outdoor conditions (Fig. 4). Since $T_s - T_a$ drives convective turbulence in the atmospheric surface layer, Fig. 4 confirms that atmospheric turbulence weakens the kinetic fractionation of water evaporation. We found that ε_k was weakly correlated with humidity h ($r = 0.34$, $p = 0.23$) and friction velocity u_* ($r = 0.32$, $p = 0.26$), the latter of which is a measure of mechanic turbulence. A stepwise linear regression using $T_s - T_a$, h, and u_* as predictors reveals that ε_k was only independently related to $T_s - T_a$, suggesting that convective turbulence played a more dominant role than mechanic turbulence in controlling the kinetic effect during our experimental trials.

The extremely high ε_k of 22.1 ‰ from Experiment B3 occurred at a very low water-to-air temperature gradient (0.25 °C, Fig. 4). The corresponding turbulence parameter n is 0.78, indicating that the level of turbulence during this experiment was almost negligible. This n value is higher than those reported for the outdoor pan evaporation experiments carried out by Craig et al. (1963) ($n = 0.50$) and Skrzypek et al. (2015) ($n = 0.40$) and even higher than most of the evaporation experiments conducted in controlled conditions. For example, Cappa et al. (2003) reported that n ranges from 0.36 to 0.44 using small evaporation dishes housed in a dynamic chamber. Using a similar flow-through evaporation chamber setup, Kim and Lee (2011) reported n values of 0.55 to 0.75. Of the 29 laboratory and natural experiments analyzed by Gonfiantini et al. (2018), only six have $n > 0.78$ and all the exceptions involve a setup where water vaporizes into quiescent air or involving a special gas. It appears that conditions during Experiment B3 were anomalous. For these reasons, the high ε_k value from Experiment B3 has been excluded from the mean value in Fig. 5 and Table 4.

4.3. Relationship between the LEL slope and kinetic fractionation

A well-known consequence of kinetic fractionation is the deviation of the local evaporation line (LEL) from the global mean meteorite water line (GMWL). The LEL is formed in a scatter plot between the hydrogen and oxygen isotope compositions of the evaporating water. Compared to the GMWL slope of 8, the LEL has a smaller slope value. Because the LEL preserves the cumulative influence of water evaporation, it is often used to help infer local hydrological conditions during the evaporation season. Gibson et al. (2008) approximated the local precipitation isotope value with the intercept of the observed LEL and the GMWL. Gibson et al. (2005) used the deviation of the LEL from the GMWL in their model to determine the watershed evaporation to inflow ratio. Skrzypek et al. (2015) estimated the water vapor isotope delta using the isotope composition of rainfall and the slope of LEL. Wassenaar et al. (2011) used the LEL slope to determine relative humidity which is a parameter required for computing the evaporation to inflow ratio. The analysis of an isotope dataset collected at a peatland stream network suggests that the LEL slope is indicative of potential evaporation (Sprenger et al., 2017). These applications generally use the default lake kinetic factor of 14.2 ‰ for ^{18}O.

The observed LEL slope is given in Table 3. Here the LEL slope was the slope of linear regression of the δ^2H value against the δ^{18}O value of the pan water. The kinetic factor itself was poorly correlated with the slope ($r = –0.05$). The correlation between $(1– h)\ \varepsilon_k$ and the slope was also weak ($r = –0.02$).

We deployed two predictive models to further examine the relationship of the LEL slope to kinetic fractionation. The first model (Model 1) is given by

Table 4
Summary of kinetic factor for ^{18}O from natural experiments. IMB: isotopic mass balance; UCG: unified Craig-Gordon model; SIMB: simplified form of IMB for terminal lakes; GD: gradient-diffusion.

Type	Area	ε_k (‰)	Method	Data source
Small water body				
Small Pan	0.13 m^2	7.01	IMB	This study
Big Pan	1.20 m^2	10.39	IMB	This study (excluding B3)
Fishpond	6900 m^2	10.17	IMB	This study
Evap Pan G	0.36 m^2	14.20	UCG	Craig et al. (1963); Gonfiantini et al. (2018)
Evap Pan S	1.13 m^2	11.36	UCG	Skrzypek et al. (2015); Gonfiantini et al. (2018)
Lake Gara	160 m^2	8.52	UCG	Fontes and Gonfiantini (1967); Gonfiantini et al. (2018)
Lake Waid	0.22 km^2	5.86	SIMB	Zimmermann (1979); Zuber (1983); Appendix A
Mean ± 1 SD		**9.64 ± 2.80**		
Large water body				
Lake Burdur	250 km^2	11.93	SIMB	Dincer (1968); Zuber (1983); Appendix A
Lake Taihu	2400 km^2	8.26	GD	Xiao et al. (2017)
Mean ± 1 SD		**10.10 ± 2.60**		

$$S_{LEL} = \frac{[\varepsilon_{eq} + (1-h)\varepsilon_k]_2}{[\varepsilon_{eq} + (1-h)\varepsilon_k]_{18}} \quad (9)$$

where subscript 2 and 18 denote ^{2}H and ^{18}O, respectively (Gat, 2010; Brooks et al., 2014). This model assumes that the evaporating water and the atmospheric vapor are in isotopic equilibrium and consequently only equilibrium fractionation and kinetic fractionation control the LEL slope. The second model (Model 2) takes a more general form (Gibson et al., 2008),

$$S_{LEL} = \frac{\left[\frac{h(\delta_V - \delta_{L,0}) + (1+10^{-3}\delta_{L,0})[(1-h)\varepsilon_k + \alpha_{eq}^{-1}\varepsilon_{eq}]}{10^3 h - (1-h)\varepsilon_k + \alpha_{eq}^{-1}\varepsilon_{eq}}\right]_2}{\left[\frac{h(\delta_V - \delta_{L,0}) + (1+10^{-3}\delta_{L,0})[(1-h)\varepsilon_k + \alpha_{eq}^{-1}\varepsilon_{eq}]}{10^3 h - (1-h)\varepsilon_k + \alpha_{eq}^{-1}\varepsilon_{eq}}\right]_{18}} \quad (10)$$

This model applies to situations where the evaporating water comes from local precipitation, and no isotopic equilibrium is assumed. Here, the δ_P in the original model was replaced by the isotopic composition of the liquid water at the start of the pan experiment ($\delta_{L,0}$). The model calculations were repeated three times using three sets of kinetic factors and were compared with the observed LEL slope (Fig. 7). The first set (solid symbols, Fig. 7) used the ^{18}O ε_k determined by isotopic mass balance (IMB; Table 3) and the ^{2}H ε_k obtained with Eq. (8) and the IMB n value in Table 3. The second set (open symbols, Fig. 7) used the lake default ε_k of 14.2 ‰ for ^{18}O and 12.5 ‰ for ^{2}H. The third set (grey symbols, Fig. 7) deployed the IMB ε_k for ^{18}O and the lake default value for ^{2}H. The fishpond experiments were excluded from this analysis because the range of the observed liquid water isotopic composition was too small during each experimental period (< 0.7 ‰ for ^{18}O) and the resulting LEL slope was too uncertain.

Both models were sensitive to how the kinetic factors were specified. Using the measured ε_k values, the modeled LEL slope was 5.52 ± 0.56 (mean ± 1 standard deviation) according to Model 1 and 4.75 ± 0.98 according to Model 2. Using the default lake ε_k values, the modeled slope was reduced to 4.71 ± 0.45 according to Model 1 and 3.89 ± 0.58 according to Model 2. The sensitivity arose mostly from changes in the kinetic factor for ^{18}O. By changing the ^{2}H kinetic factor to the default lake value but keeping the measured value for ^{18}O, the modeled slope only changed slightly, to 5.72 ± 0.75 and 5.09 ± 1.26 according to Model 1 and Model 2, respectively. Using the default lake ε_k values, Xiao et al. (2017) found that the δ_E calculated by the Craig-Gordon model falls on a LEL with a slope of about 3.2 for Lake Taihu, which is lower than the observed slope of 6.33. By switching to the lower OS kinetic factors, their calculated δ_E falls on the observed LEL.

The LEL slope predicted by Model 2 broadly agreed with the observed value (mean bias = –0.15, RMSE = 1.04), but the slope predicted by Model 1 was biased high and was more scattered (mean bias = 0.59, RMSE = 1.25). Gibson et al. (2008) found that Model 2 can reproduce the observed LEL slope for lakes in the world. The superior performance of Model 2 over Model 1 implies that although the kinetic effect plays an important role in determining the LEL slope, other factors, such as the isotopic compositions of water vapor and local water input, can also influence the slope value.

4.4. Dependence of kinetic factor on lake size

Table 4 provides a summary of the kinetic factors for ^{18}O obtained in natural conditions. They include three values from this study, four values found in the published literature, and two additional values we determined with local hydrological data reported by other authors. A range of methods were used to obtain these values, including isotopic mass balance (Small Pan, Big Pan, Fishpond), the unified Craig-Gordon model (Evap Pan G, Evap Pan S, and Lake Gara), gradient-diffusion (Lake Taihu), and simplified isotopic mass balance for terminal lakes (Lake Waid and Lake Burdur; Appendix A). Here, the ε_k value for Lake Taihu was obtained by tuning it so the Craig-Gordon model prediction matches the δ_E determined with the gradient-diffusion method and was slightly higher than that given by Xiao et al. (2017) using the wind parameterization of Merlivat and Jouzel (1979). The survey results are separated into two size classes.

According to this survey, there is no significant relationship between ε_k and lake size. The mean ε_k (^{18}O) value (9.64 ± 2.80 ‰) for the small class is not significantly different from the mean value (10.10 ± 2.60 ‰) for the large class (p = 0.85, t = –0.20, two-tailed student-t test). The overall mean ε_k is 9.74 ± 2.60 ‰ for ^{18}O, based on the 9 values in Table 4. The corresponding turbulent parameter n is 0.34. Combining this n value with Eq. (8) yields a mean kinetic factor of 8.5 ‰ for ^{2}H.

The insignificant difference in ε_k between the two size classes is based on a small data sample. More field research is needed to further evaluate this relationship. There are, however, reasons to believe that the insensitivity of ε_k to lake size may hold broadly for globe lakes. This is because wind speed and the thermal gradient in the surface layer air have opposite relationships with lake size. The longer fetch at a larger lake allows wind speed to build up, which will reduce ε_k according to the OS parameterization of Merlivat and Jouzel (1979). In a modeling study

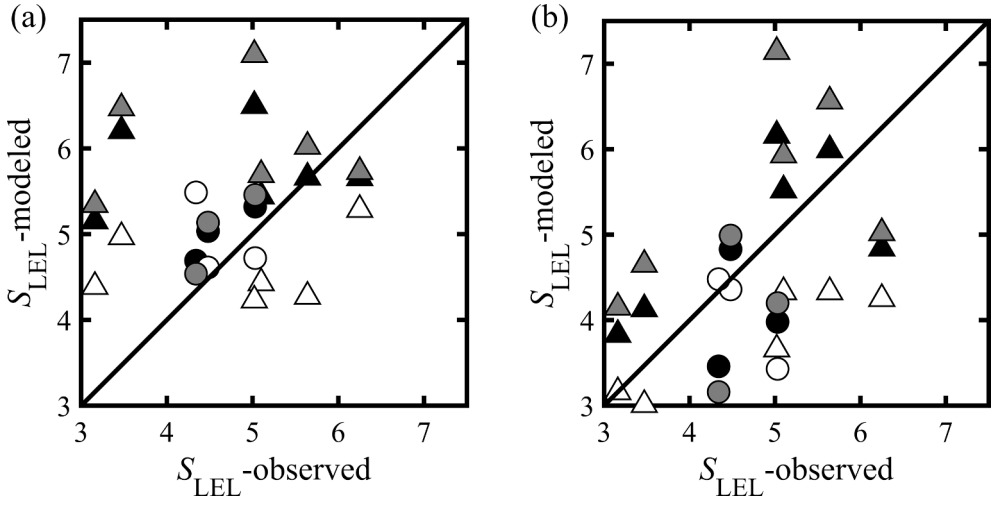

Fig. 7. Comparison of the observed LEL slope with that calculated by Eq. (9) (panel a) and Eq. (10) (panel b) using measured ε_k for ^{18}O and ^{2}H (solid symbols), default lake ε_k for ^{18}O and ^{2}H (open symbols), and the observed ε_k for ^{18}O and default lake ε_k for ^{2}H (grey symbols). Triangles denote the small evaporation pan and circles denote the big evaporation pan.

of heat diffusion between the lake and the atmosphere, Hondzo and Stefan (1993) parameterized wind speed as a proportion to lake area, increasing by about 50 % from a size of 0.01 km^2 to a size of 100 km^2. On the other hand, the water–air temperature difference $T_s - T_a$ should decrease with increasing lake size, which will result in an increase in ε_k according to Fig. 4 and may cancel out part or all of the decrease in ε_k due to the wind effect. Large lakes are generally deeper than small lakes (Cael et al., 2017) and do not warm up as fast in the evaporation season. They also tend to have lower dissolved organic carbon concentrations (Hanson et al., 2007), allowing sunlight to penetrate deeper in the water and leading to lower surface temperature, than small lakes. The inverse relationship between $T_s - T_a$ and lake size is supported by the *meta*-analysis of thermal conditions of global lakes showing that the occurrence frequency of unstable stratification in the surface layer air (Woolway et al., 2017) and the diel air temperature range (Woolway et al., 2016) are negatively correlated with lake size. Oswald and Rouse (2004) provided a numerical example on the opposing effects of lake size on wind speed and on the temperature gradient. They showed that Skeeter Lake, a small lake (area 0.05 km^2) in Northwest Territories, Canada, displayed a larger $T_s - T_a$ (4.5 °C) but lower wind speed (2.8 m s^{-1}) than Sleepy Dragon Lake, a large lake (area 5.5 km^2) in the same region ($T_s - T_a$ of 2.5 °C, wind speed of 4.2 m s^{-1}) during an ice-free season.

5. Conclusions

The kinetic factor ε_k for ^{18}O varied in the range of 2.40 ‰ to 22.10 ‰ during our experiments. The mean value was 9.70 ‰ with all the data included and 8.75 ‰ with the B3 outlier excluded. We showed that ε_k decreased linearly with increasing lake surface-to-air temperature gradient. The novelty of this finding, interpreted together with the classic parameterization of ε_k as a function of wind speed (Merlivat and Jouzel, 1979), is that the role of turbulence in kinetic fractionation manifests in both mechanic turbulence (as measured by wind speed) and convective turbulence (as measured by the temperature gradient). Although the measured ε_k showed poor correlation with the slope of the LEL (local evaporation line), it greatly improved the performance of the LEL model of Gibson et al. (2008), supporting the robustness of our isotopic mass balance method and indicating that in addition to the kinetic effect, the isotopic compositions of water vapor and local water input can also influence the LEL slope.

The ε_k data reported here and those found in the literature do not support the hypothesis that ε_k decreases with increasing lake size. The lack of sensitivity to lake size may be a result of opposing effects of lake size on wind speed and on the lake-to-air temperature gradient. The overall mean ε_k was 9.7 ‰ for ^{18}O and 8.5 ‰ for ^{2}H, based on ten outdoor experimental results covering a size range from 0.13 m^2 to 2400 km^2.

Declaration of Competing Interest

The authors declare that they have no known competing financial interests or personal relationships that could have appeared to influence the work reported in this paper.

Acknowledgments

This work was supported by the National Key R&D Program of China (Grant 2019YFA0607202 to WX) and the National Natural Science Foundation of China (Grants 41975143, 41475141, 41830860 and 42021004 to WX and MZ).

Appendix A:. Kinetic fractionation of terminal lakes

Terminal lakes are lakes that do not have surface outflows. In the special case where groundwater contribution and seepage are negligible, the water input (inflow plus precipitation) is balanced by evaporation loss, and the isotopic value of the input water is balanced by that of evaporation. Under these conditions, Poulin et al. (2019) have derived an expression for the lake water isotopic value from isotopic mass balance. Manipulating their Eq. (7), we obtain an equation for the kinetic factor, as

$$\varepsilon_k = \frac{\alpha_{eq}^{-1}\delta_L - h\delta_V - \varepsilon_{eq} - (1-h)\delta_I}{(1-h)\left(10^{-3}\delta_I + 1\right)} \quad (A.1)$$

Eq. (A.1) was used to estimate the ^{18}O kinetic factor for Lake Waid (Zimmermann, 1979; Zuber, 1983) and Lake Burdur (Dincer, 1968; Zuber, 1983). The input variables are summarized as follows:

Lake Waid, Germany

$\delta_L = -2.19$ ‰
$\delta_I = -7.91$ ‰
$\delta_V = -17.4$ ‰
$T_w = 11.1$ °C (water temperature)
$T_a = 10.55$ °C (air temperature)
$h = 0.69$ (in reference to water temperature)

Lake Burdur, Turkey

$\delta_I = -8.9$ ‰
$\delta_L = 0.3$ ‰ (Table 4 of Dincer, 1968)
$T_L = 12.9$ °C
$h = 0.59$
$\delta_V = -19.0$ ‰ (on the assumption that it is in equilibrium with δ_I (δ_P) at temperature of 12.9 °C)

Appendix B. Supplementary data

Supplementary data to this article can be found online at https://doi.org/10.1016/j.jhydrol.2021.126974.

References

Alvarez, V.M., González-Real, M.M., Baille, A., Maestre Valero, J.F., Gallego Elvira, B., 2008. Regional assessment of evaporation from agricultural irrigation reservoirs in a semiarid climate. Agric. Water Manage. 95 (9), 1056–1066. https://doi.org/10.1016/j.agwat.2008.04.003.

Arnoux, M., Barbecot, F., Gibert-Brunet, E., Gibson, J., Noret, A., 2017. Impacts of changes in groundwater recharge on the isotopic composition and geochemistry of seasonally ice-covered lakes: insights for sustainable management. Hydrol. Earth Syst. Sci. 21 (11), 5875–5889. https://doi.org/10.5194/hess-21-5875-2017.

Assouline, S., Li, D., Tyler, S., Tanny, J., Cohen, S., Bou-Zeid, E., Parlange, M., Katul, G. G., 2016. On the variability of the Priestley-Taylor coefficient over water bodies. Water Resour. Res. 52 (1), 150–163. https://doi.org/10.1002/2015WR017504.

Bello, R., Smith, J.D., 1990. The effect of weather variability on the energy balance of a lake in the Hudson Bay lowlands, Canada. Arctic Alpine Res. 22 (1), 98–107. https://doi.org/10.2307/1551724.

Benetti, M., Reverdin, G., Pierre, C., Merlivat, L., Risi, C., Steen-Larsen, H.C., Vimeux, F., 2014. Deuterium excess in marine water vapor: dependency on relative humidity and surface wind speed during evaporation. J. Geophys. Res. Atmos. 119 (2), 584–593. https://doi.org/10.1002/2013JD020535.

Berg, M.D., Popescu, S.C., Wilcox, B.P., Angerer, J.P., Rhodes, E.C., McAlister, J., Fox, W. E., 2016. Small farm ponds: overlooked features with important impacts on watershed sediment transport. J. Am. Water Resour. Assoc. 52 (1), 67–76. https://doi.org/10.1111/1752-1688.12369.

Brooks, J.R., Gibson, J.J., Birks, S.J., Weber, M.H., Rodecap, K.D., Stoddard, J.L., 2014. Stable isotope estimates of evaporation: inflow and water residence time for lakes across the United States as a tool for national lake water quality assessments. Limnol. Oceanogr. 59 (6), 2150–2165. https://doi.org/10.4319/lo.2014.59.6.2150.

Cael, B.B., Heathcote, A.J., Seekell, D.A., 2017. The volume and mean depth of Earth's lakes. Geophys. Res. Lett. 44 (1), 209–218. https://doi.org/10.1002/2016GL071378.

Cappa, C.D., Hendricks, M.B., DePaolo, D.J., Cohen, R.C., 2003. Isotopic fractionation of water during evaporation. J. Geophys. Res. Atmos. 108 (D16), 4525. https://doi.org/10.1029/2003JD003597.

Carvajal, F., Agüera, F., Sánchez-Hermosilla, J., 2014. Water balance in artificial on-farm agricultural water reservoirs for the irrigation of intensive greenhouse crops. Agric. Water Manage. 131, 146–155. https://doi.org/10.1016/j.agwat.2013.09.006.

Craig, H., Gordon, L.I., Horibe, Y., 1963. Isotopic exchange effects in the evaporation of water: 1. Low-temperature experimental results. J. Geophys. Res. 68 (17), 5079–5087. https://doi.org/10.1029/JZ068i017p05079.

Craig, H., Gordon, L.I., 1965. Deuterium and oxygen-18 variations in the ocean and the marine atmosphere. In Stable Isotopes in Oceanographic Studies and Paleotemperatures, Spoleto, Italy.

Crawford, J., Azcurra, C.S., CatherineHughes, E., Gibson, J.J., Parkes, S.D., 2019. Comparison of atmospheric water vapour $\delta^{18}O$ and $\delta^{2}H$ estimated using evaporation pan, rainfall equilibrium and continuous measurements. J. Hydrol. 576, 551–560. https://doi.org/10.1016/j.jhydrol.2019.06.056.

Devi, P., Jain, A.K., Rao, M.S., Kumar, B., 2015. Isotopic composition of atmospheric moisture from pan water evaporation measurements. Isotopes Environ. Health Stud 51 (3), 426–438. https://doi.org/10.1080/10256016.2015.1037301.

Dincer, T., 1968. The use of oxygen 18 and deuterium concentrations the water balance lakes. Water Resour. Res. 4 (6), 1289–1306. https://doi.org/10.1029/WR004i006p01289.

Downing, J.A., Prairie, Y.T., Cole, J.J., Duarte, C.M., Tranvik, L.J., Striegl, R.G., McDowell, W.H., Kortelainen, P., Caraco, N.F., Melack, J.M., Middelburg, J.J., 2006. The global abundance and size distribution of lakes, ponds, and impoundments. Limnol. Oceanogr. 51 (5), 2388–2397. https://doi.org/10.4319/lo.2006.51.5.2388.

Feng, X., Lauder, A.M., Posmentier, E.S., Kopec, B.G., Virginia, R.A., 2016. Evaporation and transport of water isotopologues from Greenland lakes: the lake size effect. Quat. Sci. Rev. 131 (B1), 302–315. https://doi.org/10.1016/j.quascirev.2015.07.029.

Finger Higgens, R.A., Chipman, J.W., Lutz, D.A., Culler, L.E., Virginia, R.A., Ogden, L.A., 2019. Changing lake dynamics indicate a drier Arctic in western Greenland. J. Geophys. Res. Biogeosci. 124 (4), 870–883. https://doi.org/10.1029/2018JG004879.

Fontes, J.-C., Gonfiantini, R., 1967. Comportement isotopique au cours de l'évaporation de deux bassins sahariens (Isotopic behaviour of two Saharian ponds during evaporation). Earth Plan. Sci. Letters 3, 258–266. https://doi.org/10.1016/0012-821X(67)90046-5 and 386 (errata).

Fowler, K., Morden, R., Lowe, L., Nathan, R., 2015. Advances in assessing the impact of hillside farm dams on streamflow. Australasian J. Water Resour. 19 (2), 96–108. https://doi.org/10.1080/13241583.2015.1116182.

Gat, J.R., Bowser, C.J., Kendall, C., 1994. The contribution of evaporation from the Great Lakes to the continental atmosphere: estimate based on stable isotope data. Geophys. Res. Lett. 21 (7), 557–560. https://doi.org/10.1029/94GL00069.

Gat, J.R., 2010. Isotope Hydrology: A Study of the Water Cycle. Imperial College Press.

Gibson, J.J., Birks, S.J., Edwards, T.W.D., 2008. Global prediction of δ_A and $\delta^{2}H$-$\delta^{18}O$ evaporation slopes for lakes and soil water accounting for seasonality. Glob. Biogeochem. Cycle 22 (2), GB2031. https://doi.org/10.1029/2007GB002997.

Gibson, J.J., Birks, S.J., Yi, Y., Moncurc, M.C., McEachernd, P.M., 2016. Stable isotope mass balance of fifty lakes in central Alberta: Assessing the role of water balance parameters in determining trophic status and lake level. J. Hydrol. Regional Stud. 6, 13–25. https://doi.org/10.1016/j.ejrh.2016.01.034.

Gibson, J.J., Edwards, T.W.D., Birks, S.J., St Amour, N.A., Buhay, W.M., McEachern, P., Wolfe, B.B., Peters, D.L., 2005. Progress in isotope tracer hydrology in Canada. Hydrol. Process. 19 (1), 303–327. https://doi.org/10.1002/hyp.5766.

Gonfiantini, R., 1986. Environmental isotopes in lake studies. Handbook of environmental isotope geochemistry. Terrestrial Environ. 113–168.

Gonfiantini, R., Wassenaar, L.I., Araguas-Araguas, L.J., Aggarwal, P.K., 2018. A unified Craig-Gordon isotope model of stable hydrogen and oxygen isotope fractionation during fresh or saltwater evaporation. Geochim. Cosmochim. Acta 235, 224–236. https://doi.org/10.1016/j.gca.2018.05.020.

Gonfiantini, R., Wassenaar, L.I., Araguas-Araguas, L.J., 2020. Stable isotope fractionations in the evaporation of water: the wind effect. Hydrol. Process. 34 (16), 3596–3607. https://doi.org/10.1002/hyp.13804.

Guo, X., Liu, H., Yang, K., 2015. On the application of the Priestley-Taylor relation on sub-daily time scales. Bound.-Layer Meteorol. 156, 489–499. https://doi.org/10.1007/s10546-015-0031-y.

Habets, F., Molenat, J., Carluer, N., Douez, O., Leenhardt, D., 2018. The cumulative impacts of small reservoirs on hydrology: a review. Sci. Total Environ. 643, 850–867. https://doi.org/10.1016/j.scitotenv.2018.06.188.

Hanson, P.C., Carpenter, S.R., Cardille, J.A., Coe, M.T., Winslow, L.A., 2007. Small lakes dominate a random sample of regional lake characteristics. Freshw. Biol. 52 (5), 814–822. https://doi.org/10.1111/j.1365-2427.2007.01730.x.

Hellmann, R., Harvey, A.H., 2020. First-principles diffusivity ratios for kinetic isotope fractionation of water in air. Geophys. Res. Lett. 47 (18), e2020GL089999 https://doi.org/10.1029/2020GL089999.

Hondzo, M., Stefan, H.G., 1993. Regional water temperature characteristics of lakes subjected to climate change. Clim. Change 24, 187–211. https://doi.org/10.1007/BF01091829.

Jasechko, S., Gibson, J.J., Edwards, T.W.D., 2014. Stable isotope mass balance of the Laurentian Great Lakes. J. Great Lakes Res. 40 (2), 336–346. https://doi.org/10.1016/j.jglr.2014.02.020.

Kaimal, J.C., Finnigan, J.J., 1994. Atmospheric Boundary Layer Flows: Their Structure and Measurement. Oxford University Press.

Kim, K., Lee, X., 2011. Isotopic enrichment of liquid water during evaporation from water surfaces. J. Hydrol. 399 (3-4), 364–375. https://doi.org/10.1016/j.jhydrol.2011.01.008.

Maberly, S.C., O'Donnell, R.A., Woolway, R.I., Cutler, M.E.J., Gong, M., Jones, I.D., Merchant, C.J., Miller, C.A., Politi, E., Scott, E.M., Thackeray, S.J., Tyler, A.N., 2020. Global lake thermal regions shift under climate change. Nat. Commun. 11, 1232. https://doi.org/10.1038/s41467-020-15108-z.

Merlivat, L., Jouzel, J., 1979. Global climatic interpretation of the deuterium-oxygen 18 relationship for precipitation. J. Geophys. Res. Oceans 84 (C8), 5029–5033. https://doi.org/10.1029/JC084iC08p05029.

Merlivat, L., 1978. Molecular diffusivities of $H_2{}^{16}O$, $HD^{16}O$, and $H_2{}^{18}O$ in gases. J. Chem. Phys. 69 (6), 2864–2871. https://doi.org/10.1063/1.436884.

Messager, M.L., Lehner, B., Grill, G., Nedeva, I., Schmitt, O., 2016. Estimating the volume and age of water stored in global lakes using a geo-statistical approach. Nat. Commun. 7, 13603. https://doi.org/10.1038/ncomms13603.

Moore, C.J., 1986. Frequency response corrections for eddy correlation systems. Bound.-Layer Meteorol. 37, 17–35. https://doi.org/10.1007/BF00122754.

Oswald, C.J., Rouse, W.R., 2004. Thermal characteristics and energy balance of various-size Canadian shield lakes in the Mackenzie River Basin. J. Hydrometeorol. 5 (1), 129–144. https://doi.org/10.1175/1525-7541(2004)005<0129:TCAEBO>2.0.CO;2.

Poulin, C., Hamelin, B., Vallet-Coulomb, C., Amngar, G., Loukman, B., Cretaux, J.F., Doumnang, J.C., Nour, A.M., Menot, G., Sylvestre, F., Deschamps, P., 2019. Unraveling the hydrological budget of isolated and seasonally contrasted subtropical lakes. Hydrol. Earth Syst. Sci. 23, 1705–1724. https://doi.org/10.5194/hess-23-1705-2019.

Priestley, C.H.B., Taylor, R.J., 1972. On the assessment of surface heat flux and evaporation using large-scale parameters. Mon. Weather Rev. 100 (2), 81–92. https://doi.org/10.1175/1520-0493(1972)100<0081:OTAOSH>2.3.CO;2.

Scheffer, M., Van Geest, G.J., Zimmer, K., Jeppesen, E., Sondergaard, M., Butler, M.G., Hanson, M.A., Declerck, S., De Meester, L., 2006. Small habitat size and isolation can promote species richness: second-order effects on biodiversity in shallow lakes and ponds. Oikos 112 (1), 227–231. https://doi.org/10.1111/j.0030-1299.2006.14145.x.

Skrzypek, G., Mydłowski, A., Dogramaci, S., Hedley, P., Gibson, J.J., Grierson, P.F., 2015. Estimation of evaporative loss based on the stable isotope composition of water using Hydrocalculator. J. Hydrol. 523, 781–789. https://doi.org/10.1016/j.jhydrol.2015.02.010.

Sprenger, M., Tetzlaff, D., Tunaley, C., Dick, J., Soulsby, C., 2017. Evaporation fractionation in a peatland drainage network affects stream water isotope composition. Water Resour. Res. 53 (1), 851–866. https://doi.org/10.1002/2016WR019258.

Stewart, R.B., Rouse, W.R., 1976. A simple method for determining the evaporation from shallow lakes and ponds. Water Resour. Res. 12 (4), 623–628. https://doi.org/10.1029/WR012i004p00623.

Verpoorter, C., Kutser, T., Seekell, D.A., Tranvik, L.J., 2014. A global inventory of lakes based on high-resolution satellite imagery. Geophys. Res. Lett. 41 (18), 6396–6402. https://doi.org/10.1002/2014GL060641.

Wang, Y., Wang, X., Wu, Q., Chen, C., Xu, A., Ding, P., 2018. The small-island effect in amphibian assemblages on subtropical land-bridge islands of an inundated lake. Curr. Zool. 64 (3), 303–309. https://doi.org/10.1093/cz/zox038.

Wassenaar, L.I., Athanasopoulos, P., Hendry, M.J., 2011. Isotope hydrology of precipitation, surface and ground waters in the Okanagan Valley, British Columbia, Canada. J. Hydrol. 411 (1-2), 37–48. https://doi.org/10.1016/j.jhydrol.2011.09.032.

Wen, X.-F., Sun, X.-M., Zhang, S.-C., Yu, G.-R., Sargent, S.D., Lee, X., 2008. Continuous measurement of water vapor D/H and $^{18}O/^{16}O$ isotope ratios in the atmosphere. J. Hydrol. 349 (3-4), 489–500. https://doi.org/10.1016/j.jhydrol.2007.11.021.

Woolway, R.I., Jones, I.D., Maberly, S.C., French, J.R., Livingstone, D.M., Monteith, D.T., Simpson, G.L., Thackeray, S.J., Andersen, M.R., Battarbee, R.W., DeGasperi, C.L., Evans, C.D., de Eyto, E., Feuchtmayr, H., Hamilton, D.P., Kernan, M., Krokowski, J., Rimmer, A., Rose, K.C., Rusak, J.A., Ryves, D.B., Scott, D.R., Shilland, E.M., Smyth, R.L., Staehr, P.A., Thomas, R., Waldron, S., Weyhenmeyer, G.A., Miller, T., 2016. Diel surface temperature range scales with lake size. PLoS One 11 (3), e0152466. https://doi.org/10.1371/journal.pone.0152466.

Woolway, R.I., Verburg, P., Merchant, C.J., Lenters, J.D., Hamilton, D.P., Brookes, J., Kelly, S., Hook, S., Laas, A., Pierson, D., Rimmer, A., Rusak, J.A., Jones, I.D., 2017. Latitude and lake size are important predictors of over-lake atmospheric stability. Geophys. Res. Lett. 44 (17), 8875–8883. https://doi.org/10.1002/2017GL073941.

Xiao, K., Griffis, T.J., Baker, J.M., Bolstad, P.V., Erickson, M., Lee, X., Wood, J.D., Hu, C., Nieber, J.L., 2018. Evaporation from a temperate closed-basin lake and its impact on present, past, and future water level. J. Hydrol. 561, 59–75. https://doi.org/10.1016/j.jhydrol.2018.03.059.

Xiao, W., Lee, X., Hu, Y., Liu, S., Wang, W., Wen, X., Werner, M., Xie, C., 2017. An experimental investigation of kinetic fractionation of open-water evaporation over a large lake. J. Geophys. Res. Atmos. 122 (21), 11651–11663. https://doi.org/10.1002/jgrd.v122.2110.1002/2017JD026774.

Xiao, W., Zhang, Z., Wang, W., Zhang, M., Liu, Q., Hu, Y., Huang, W., Liu, S., Lee, X., 2020. Radiation controls the interannual variability of evaporation of a subtropical lake. J. Geophys. Res. Atmos. 125, e2019JD031264 https://doi.org/10.1029/2019JD031264.

Yao, J., Zhao, Y., Yu, X., 2018. Spatial-temporal variation and impacts of drought in Xinjiang (Northwest China) during 1961–2015. PeerJ 6, e4926. https://doi.org/10.7717/peerj.4926.

Zhao, J., Zhang, M., Xiao, W., Wang, W., Zhang, Z., Yu, Z., Xiao, Q., Cao, Z., Xu, J., Zhang, X., Liu, S., Lee, X., 2019. An evaluation of the flux-gradient and the eddy covariance method to measure CH_4, CO_2, and H_2O fluxes from small ponds. Agric. For. Meteorol. 275, 255–264. https://doi.org/10.1016/j.agrformet.2019.05.032.

Zimmermann, U., 1979. Determination by stable isotopes of underground inflow and outflow and evaporation of young artificial groundwater lakes. In: Isotopes in Lake Studies. Int. At. Energy Agency (I.A.E.A.), Vienna, pp. 87–94.

Zuber, A., 1983. On the environmental isotope method for determining the water balance components of some lakes. J. Hydrol. 61 (4), 409–427. https://doi.org/10.1016/0022-1694(83)90004-5.